In vitro and *in silico* evaluation of the anti-inflammatory and anti-amyloid properties of curcumin and a V (IV) – curcumin complex in LPS-challenged primary rat neuron-microglia mixed cultures

Georgios Katsipis[a,b], Sophia Lavrentiadou[b,d*], George D. Geromichalos[b,c], Maria Tsantarliotou[d], Eleni E. Tzekaki[a,b], Eleftherios Halevas[a,e], George Litsardakis[f], Anastasia A. Pantazaki[a,b*]

[a] Laboratory of Biochemistry, Department of Chemistry, Aristotle University of Thessaloniki, 54124, Thessaloniki, Greece

[b] Center for Interdisciplinary Research and Innovation, Laboratory of Neurodegenerative Diseases (LND), 57001, Thermi, Thessaloniki, Greece

[c] Laboratory of Inorganic Chemistry, Department of Chemistry, Aristotle University of Thessaloniki, 54124, Thessaloniki, Greece

[d] Laboratory of Physiology, School of Veterinary Medicine, Aristotle University of Thessaloniki, Thessaloniki, 54124, Greece

[e] Institute of Biosciences & Applications, National Centre for Scientific Research "Demokritos", 15310, Athens, Greece

[f] Laboratory of Materials for Electrotechnics, School of Electrical and Computer Engineering, Aristotle University of Thessaloniki, 54124, Thessaloniki, Greece

*** Corresponding authors:**

Professor Dr. Anastasia A. Pantazaki, Lab. of Biochemistry, Dept. of Chemistry, Aristotle University of Thessaloniki, 54124 Thessaloniki, Greece, Tel: +30-2310-997838 & Fax: +30-2310-997689

E-mail: natasa@chem.auth.gr

Web page : https://www.chem.auth.gr/en/staff/apantazaki/

Associate Professor Dr. Sophia Lavrentiadou, Lab. of Physiology, School of Veterinary Medicine, Aristotle University of Thessaloniki, 54124 Thessaloniki, Greece, Tel: +30-2310-999872

E-mail: slavrent@vet.auth.gr

Web page : https://users.auth.gr/~slavrent/

Supplementary Materials

Index

Section S1. Culturing of primary rat mixed neuron-glia cultures

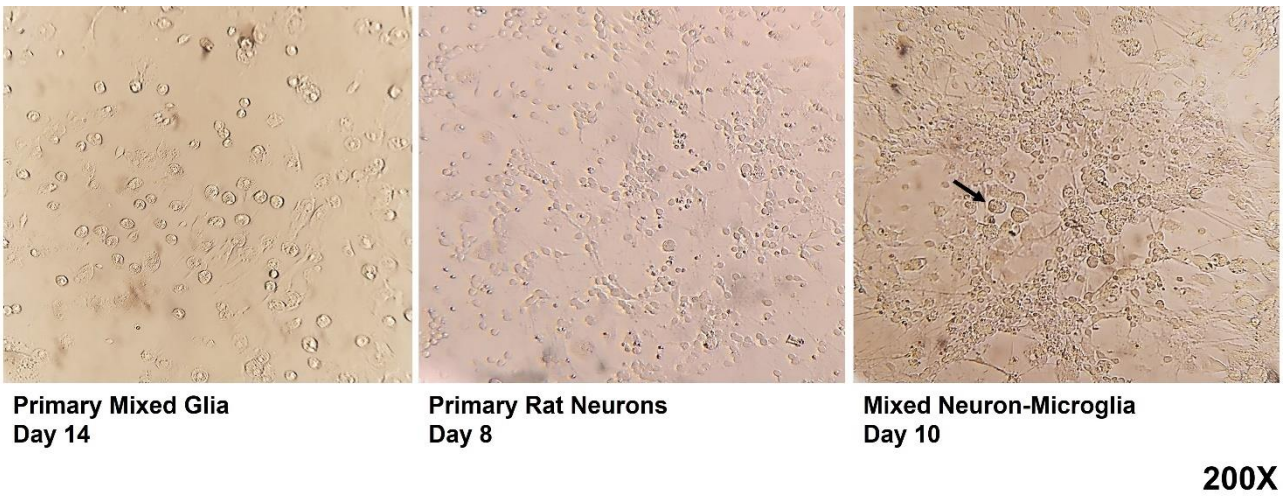

Fig. S1. Representative photos from rat primary neuronal cells isolated from neonatal brains and cultured in the current study. From left to right:14-day primary microglia, 8-day neurons and 10-day neurons after mixing with microglia on day 8. Photos were captured from an inverted microscope (200-times final magnification).

S1.1. Microscopic evaluation of mixed neurons-microglia cultures treated with LPS and/or curcumin or V-Cur

Mixed cultures of rat primary neurons and microglia 24 hours after treatment with LPS in the absence or presence of curcumin or V-Cur were observed under an inverted microscope, at 100x magnification (Fig. 2). Exposure of co-cultures to LPS, curcumin or V-Cur did not elicit any observable alterations in cell morphology. However, LPS significantly reduced the observed neurons that were cultured in the absence of microglia, while microglia were present in higher density in the LPS-treated group compared to the control group (Fig. 2). The presence of curcumin or V-Cur inhibited this increase in microglia density. Interestingly, V-Cur was precipitated on extracellular, aggregative, orange formations on the culture plates when observed under an inverted light microscope (Fig. 2). Such an effect was also found in some cases for curcumin too, but the formations were more dispersed, with weaker coloration.

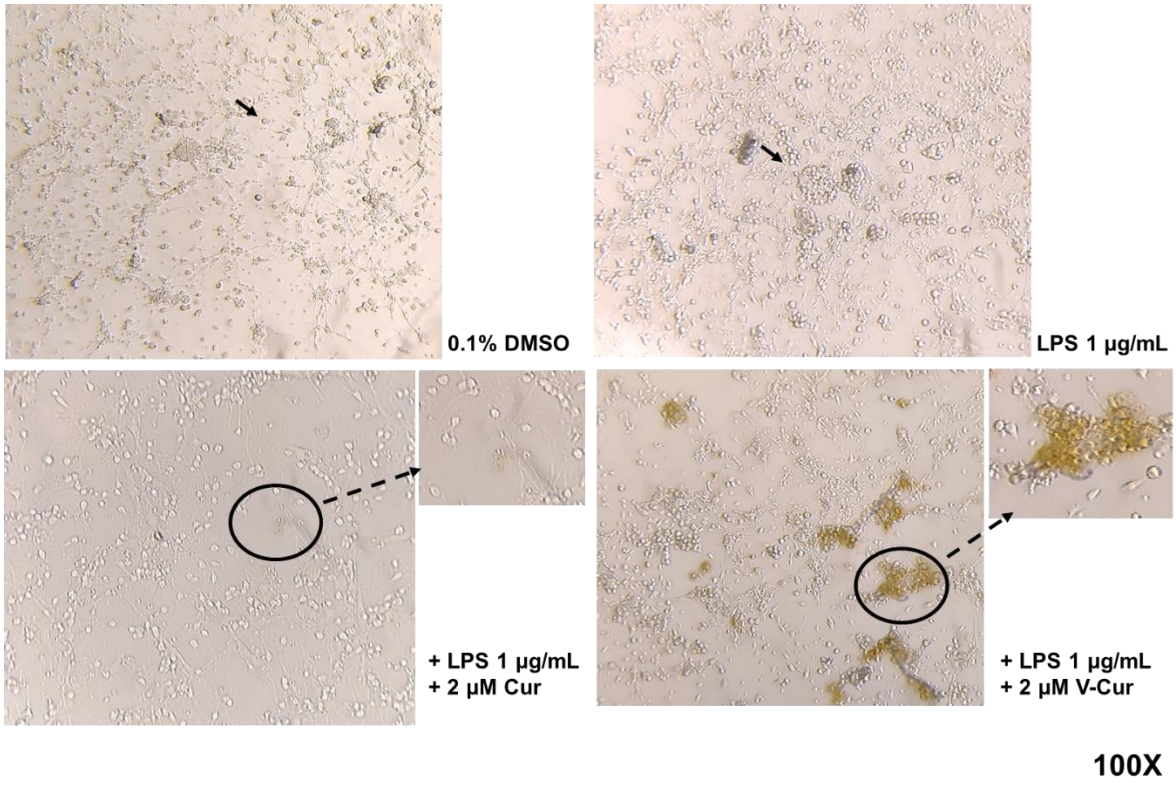

Fig. S2. Light inverted microscopy pictures of mixed cultures of primary neurons-microglia isolated from neonatal brains, at 100 X magnification, after treated with 0.1% (v/v) DMSO (Control sample), LPS 1 µg/ml, co-treated with LPS and curcumin 2 µM, and co-treated with LPS and V-Cur complex 2 µM. Picture insets: enlarged areas from the cultures treated with either curcumin or V-Cur complex, where orange aggregates/precipitates were visualized after 24 hours of treatment.

Section S2. Molecular docking calculations

S2.1. *In silico* computational methods

A series of *in silico* molecular docking studies were employed in order to predict the potential inhibitory activity of curcumin and V-Cur on iNOS, TNF-α, IL-1β, $A\beta_{1-42}$, and Aβ fibril and APP target proteins and peptides involved in the neurodegenerative pathway. The *in silico* predictive tools that have been employed to study the interactions of the compounds with the selected macromolecules, are Schrödinger, Mercury, ChemBio3D Ultra, Spartan' 14, and PyMol molecular modeling software. The 3-D structure of the synthesized vanadium/curcumin complex was generated from its X-ray crystal structure as a CIF file. Mercury software (http://www.ccdc.cam.ac.uk/) was then used to convert the CIF file to PDB format file. The structure of curcumin was retrieved by PubChem chemical information resource library at the U.S. National Center for Biotechnology Information (NCBI) (https://pubchem.ncbi.nlm.nih.gov) (CID_969516). 3D conformers of each molecular structure were optimized through energy minimization (MM2 force field method) with the aid of ChemBio3D Ultra v. 14.0.0.117 software suite (CambridgeSoft Corporation) and subsequently pdb files of each structure were generated. The best, most stable (lowest energy) conformation of the molecular model of each compound was detected by geometrical optimization in the gas phase, as implemented in the Spartan '14 Molecular Modeling program suite (Spartan '14 v.1.1.4, Wavefunction Inc., Irvine, CA, USA; www.wavefun.com.). The structures were initially optimized (*via* energy minimization) by conformational search using the Monte Carlo method with the MMFF94 molecular mechanics model, included in the Spartan'14 program suite. Geometry optimization (leading to the most stable conformer with the lowest energy) was accomplished *via* quantum-chemical calculations by utilizing Density Functional Theory (DFT) computations at B3LYP level of theory with 6-31G*(d,p) basis set to describe the accurate structural and electronic properties of the compounds, implemented by Spartan' 14 program suite.

Molecular docking calculations were carried out on the crystal structures of the target proteins iNOS, TNF-α, and IL-1β [Protein Data Bank (PDB) accession numbers: 4NOS, 2AZ5, and 1ITB, respectively] refined at 2.25 Å, 2.10 Å, and 2.50 Å, respectively. The X-ray crystallographic structures were obtained from the Brookhaven Protein Data Bank (operated by the Research Collaboratory for Structural Bioinformatics, RCSB) [1–3]. iNOS with 427 amino acid length is co-crystallized with

iron protoporphyrin IX (heme), 5,6,7,8-tetrahydrobiopterin (H_4B), dihydrobiopterin (H_2B) 2-amino-6-(1,2-dihydroxy-propyl)-7,8-dihydro-6H-pteridin-4-one, ethylisothiourea (ITU), and Zinc ion (Zn^{+2}) [4]. For the docking calculations on iNOS it was used only the A chain of the protein since chains B, C, and D, are replicates, with co-crystallized ligands bound at the same ligand binding site among the chains. For this reason, from corresponding PDB files it was deleted the data for chains B-D and also the data of the drug referring to these chains. The crystal structure of TNF-α used was the dimer protein (chains A and B were considered, while chains C and D were neglected as replicates completing the construction of the tetramer protein structure), with the co-crystallized TNF-a receptor binding inhibitor SP307 composed of trifluoromethylphenyl indole and dimethyl chromone moieties linked by a dimethylamine spacer (6,7-dimethyl-3-[(methyl{2-[methyl ({1-[3-(trifluoromethyl) phenyl]-1H-indol-3-yl} methyl)amino]ethyl}amino) methyl]-4H-chromen -4-one) [5]. For this reason, from corresponding PDB files it was deleted the data for chains C-D and also the data of the drug referring to these chains. It was also used the crystal structure of IL-1β (chain A, 153 amino acids) complexed with the type-I interleukin-1 receptor (IL-1R1) (chain B, 315 amino acids) [6]. Ligands and heteroatoms from all crystal structures were removed to clean and optimize the structures.

Molecular docking calculations were also carried out on the solution-state NMR structures of $A\beta_{1-42}$ [7], and Aβ fibril [8] target peptides (PDB accession numbers: 1IYT, 1QWP, and 2BEG, respectively), as well as on the crystal structure of the Kunitz protease inhibitor domain (APPI) of APP [9], determined and refined to 1.5 Å resolution (PDB accession number 1AAP).

The Schrödinger software suite contains a broad array of computational chemistry tools. In the procedure for molecular docking with the employment of Schrödinger suite both compounds were converted into three-dimensional MOL2 files using Schrödinger Release 2020-3 Maestro Version 11.1 and minimized using LigPrep 3.5 [10] (which can generate a number of structures from each input structure with various ionization states, tautomers, stereochemical characteristics, and ring conformations to eliminate molecules on the basis of various criteria such as molecular weight or specified numbers and types of functional groups with correct chiralities for each successfully processed input structure), and the OPLS3 (Optimized Potential for Liquid Simulations) [11] force field for the optimization, producing the low-energy isomers of the ligands (Schrödinger, http://www.schrodinger.com). Energy minimized

3D molecular structures were generated with the employment of LigPrep run from Maestro utility of the Schrödinger suite. The ligand preparation included 2D–3D conversions, generating variations, correction, verification and optimization of the structures. A preparation of receptor and ligand structures was integrated before the actual docking procedure [12]. The crystal structures of the proteins were prepared using the Protein Preparation Wizard [12], in Schrödinger Suite 2020-3 (Schrödinger, LLC, New York, NY) [13,14]. Protein was prepared by adding the hydrogen atoms, optimizing hydrogen bonds, removing atomic clashes, adding formal charges to the hetero groups and then optimizing at neutral pH. Missing loops and side chains were prepared using Prime version 3.2 [15,16]. Finally, the structure was minimized using OPLS3 force field. Active site of studied proteins was obtained using SiteMap tool (version 3.6, Schrödinger) [17], which provides a fast and effective means of identifying potential binding pockets of proteins. SiteMap identifies the character of binding sites using novel search and assesses each site by calculating various properties like size, volume, amino acid exposure, enclosure, contact, hydrophobicity, hydrophilicity and donor/acceptor ratio. Receptor grid was generated around the active site for effective binding using Receptor grid generation in the Glide (version 5.9) application of Maestro. Once the receptor grid is generated, the ligands are docked to the proteins using Glide docking tool of Schrödinger (Grid based Ligand Docking with Energetics) (version 6.8) [18]. Compounds were docked in the binding site of the proteins using Induced-Fit Docking (IFD) protocol 2020-3 [19–21]. The ligand interactions are shown in Ligand interaction tool of Maestro (Schrödinger). Waters were deleted with Maestro, the graphical user interface (GUI) of Schrödinger software, prior to docking. Molecular docking studies were carried out for the best fitted compounds to the model, while the final selection criteria were compounds docking scores and the presence of crucial interactions for binding to the studied proteins [22]. The resulting poses were examined manually, and the most promising ones were redocked with IFD calculations. Poses that pass the initial screens enter the final stage of the algorithm, which involves evaluation and minimization of a grid approximation to the OPLS-AA nonbonded ligand-receptor interaction energy. Final scoring is then carried out on the energy-minimized poses. By default, Schrödinger's proprietary Glide Score [23] multi-ligand scoring function is used to score the poses. The rescoring was performed to calculate and improved binding energy calculations with Prime's Molecular Mechanics-Generalized Born Surface Area (MM-GBSA) protocol using

VSGB solvation model [24,25]. All complexes showed good docking scores reflecting drug-binding affinities with the studied proteins. PyMol Molecular Graphics System (Schrödinger, LLC. version 2.3.5, www.pymol.org) [26] was used to visualize the molecules and analyze the results of the docking and to construct the molecular models.

S2.2. Further information on docking studies

$A\beta_{1\text{-}42}$

The binding poses of both curcumin and V-Cur (Fig. 6a) suggest anchorage in the binding pocket with the formation of contacts with the KLVFFAED sequence of the peptide (K16, L17, and F20 for curcumin and K16, F19, F20, and D23 for V-Cur) as well as binding sites before (N-terminal) and after (hinge region) KLVFFAED (V12, V24, I31, and L34 for curcumin, and V24, N27, I31, and L34 for V-Cur). Common binding residues among the two molecules were revealed to be K16, F20, V24, I31, and L34. Similar binding contacts of curcumin and curcumin derivatives are previously reported [27]. Free axial vanadate oxygen of V-Cur is also a hydrogen bond connected to D23 carboxylic Oδ1 (2.1 Å). Further stabilization of V-Cur inside the binding site of $A\beta_{1\text{-}42}$ monomer peptide is achieved by the formation of π-π stacking T-shaped contacts formed between the aromatic rings of F20 and F19 and aromatic C atoms of anisole moiety of curcumin and the 2,2′-bipyridine (bipy) of V-Cur, respectively. Other special interactions of V-Cur involve π-charge electrostatic contacts including π-anion between the negative charge of the pyridine aromatic ring of bipy moiety and the negative charge of carboxylic Oδ2 of D23 (3.0 Å) and π-cation between the negative charge of one of the anisole rings and the positive charge of Nζ of K16 (3.1 Å). Additionally, polar contacts were established between the axial vanadate O and either I31/Cδ1 or V24/Cγ2 (2.9 or 3.4 Å, respectively). Curcumin was found to be anchored in its binding site *via* the formation of π-polar contacts with F20, π-cation with K16/Nζ, π-alkyl with K16/Cε, V12/Cγ2, L34/Cδ2, and V24/Cγ2, and polar contact between the phenolic OH of anisole and I31/Cγ2 (2.4 Å). Furthermore, it has been reported [28] that there are three structural properties of interaction that can destabilize the assembly of Aβ: 1) Electrostatic interaction between residues D23-K28 forms a hydrophilic region; 2) E22 helps in maintaining the stability between chains of fibrils and helps to remain intact, and 3) Residue in between L17-A21 and A30-A42 from a hydrophobic region which

can be the target region to mask and block oligomerization. Most of these binding regions are shown to be common with those of curcumin and V-Cur.

Aβ fibril

The ligand-binding site of molecules depicting the extent of the pocket as determined by the computation process, labeling the critical residues interacting with the molecules, are shown in the upper part of Fig. 6b. Ligand interactions of curcumin and V-Cur stabilized at the β clusters formed at the concave edge of the Aβ fibril. The docking procedure predicts the formation of a variety of interactions with residues L17, F19, V40, I41, and A42 of all five chains A-E. Stabilization of both anchored compounds may be attributed to H-bond, hydrophobic, and polar contacts. Other special interactions involve π-polar and π-alkyl type hydrophobic contacts with the residues of the binding site. Interestingly, one of the binding contacts of both curcumin and V-Cur, F19, is reported to be one of the key inter-sheet contacts formed between residues of the antiparallel sheets (F19/G38).

APPI

In Fig. 6c is depicted the best-fitted anchorage of curcumin and V-Cur in the active site of APPI, labeling also the critical amino acid residue contacts. The binding interactions are reported in Table S1. The binding contacts of both compounds in the interface between chains A and B of the protein were revealed to be residues Q8, A9, Y22, D24, T26, E27, and F33 of chain A and Q8, T11, D24, V25, T26, P32, F33, and F34 of chain B (curcumin), and Q8, A9, Y22, D24, V25, and T26 of chain A and Q8, A9, T11, Y22, D24, T26, E27, P32, F33, and F34 of chain B (V-Cur). Most of the residues are shown to be common between the two molecules.

iNOS

Binding residues of either curcumin only W194, F369, and W372, or only V-Cur, Y489, and both curcumin and V-Cur M355, found to be common with that of heme (Fig. 7a). Furthermore, a binding contact of both docked molecules, E377 located adjacent to the active site, is also forming an essential bidentate interaction by its glutamate group with the inhibitor ITU. The ethyl group of ITU is shown to be packed near the heme and F369 side chain [4], which is a binding contact of curcumin. T463 common binding residue of the monomer near the dimerization interface is located on

one side of the pocket (T461 and F476 being the opposite face residues from the other monomer, not shown in the structure).

Further stabilization of both molecules in the binding pocket is achieved with the formation of π-cation and π-anion contacts between the aromatic rings of one of the anisole moieties of curcumin and V-Cur and R388/Nη1 and D382/Oδ1, E377/Oε1 atoms, respectively. Pi-cation interaction is also observed between R266/Nη1 and bipy moiety ring of V-Cur and π-polar between T121/Oγ1 and N354/Nδ2 and bipy ring, and N354/Nδ2 and N263/Nε2 and one of the anisole rings of V-Cur and π-alkyl between A262/Cβ and bipy. Additionally, the N454/NH is found to be involved in a hydrogen bond (H-bond) with one of the pyridine nitrogens of the bipy moiety and one axial vanadate oxygen atom of V-Cur. H-bond contacts were also observed between both hydroxyl anisole oxygens of V-Cur and curcumin and Y373/OH, E377/O, and C200/N, and between anisole O of curcumin and R199/N. Furthermore, both phenolic and methoxy-O atoms of anisole are hydrogen bonds connected to E377/O (2.1 Å), D382/HO2, Oδ2 (3.2, 3.1 Å), I378/N (3.7 Å), and R388/Nη1, Nη2 (3.5, 2.9 Å). Both molecules are further stabilized in the binding pocket of iNOS with the contribution of π-π stacking, displaced and T-shaped interactions between the anisole aromatic ring and the aromatic rings of W463, F369, Y373, and W346, and the bipy ring and Y491. The free axial vanadate hydroxyl group is also a hydrogen bond connected to Oδ1 of N354 (3.6 Å). Several hydrophobic contacts additionally stabilized the anchored curcumin and V-Cur molecules in the binding cavity of the enzyme.

IL-1β

The stabilization of both anchored compounds may be attributed to hydrogen bonds, hydrophobic, polar, and electrostatic contacts inside the binding pocket of the interface between the IL-1β/IL-1R1 complex. The docking procedure demonstrated the following common binding contacts between the two docked molecules: E105, N108, M148, and F150 for IL-1β, and N204 (of 90s loop), Q236, S238, and R271 for IL-1R1. The binding residues, not common for the two molecules revealed to be L6, M44, F46, I56, K103, I106, N107 (IL-1β), K205, P206, D239, I240, K298, N299, T300, and H301 (IL-1R1) for curcumin, and K109, L110, T147, Q149, S152 (IL-1β), R174, I199, T200, L201, E202, L237, E265, and K270 (IL-1R1) for V-Cur. Key binding contact residues necessary for the stabilization between IL-1β and IL-1R1 at site B, F46, and L237, respectively, are predicted to be also binding contacts of V-Cur (Table S2) Free axial

vanadate oxygen is also hydrogen bond connected to R271/Nη1H (3.9 Å), S152/OγH (3.8 Å), and F150/O, NH (2.8, 2.9 Å). In general, the identified binding pocket of V-Cur, represents a promising focus point for targeting the stabilization of the dimeric IL-1β/IL-1R1 protein structure.

References

[1] H.M. Berman, The Protein Data Bank, Nucleic Acids Res. 28 (2000) 235–242. https://doi.org/10.1093/nar/28.1.235.

[2] H. Berman, K. Henrick, H. Nakamura, Announcing the worldwide Protein Data Bank, Nat Struct Mol Biol. 10 (2003) 980–980. https://doi.org/10.1038/nsb1203-980.

[3] F.C. Bernstein, T.F. Koetzle, G.J. Williams, E.F. Meyer, M.D. Brice, J.R. Rodgers, O. Kennard, T. Shimanouchi, M. Tasumi, The Protein Data Bank: a computer-based archival file for macromolecular structures., J Mol Biol. 112 (1977) 535–42. https://doi.org/10.1016/s0022-2836(77)80200-3.

[4] T.O. Fischmann, A. Hruza, X.D. Niu, J.D. Fossetta, C.A. Lunn, E. Dolphin, A.J. Prongay, P. Reichert, D.J. Lundell, S.K. Narula, P.C. Weber, Structural characterization of nitric oxide synthase isoforms reveals striking active-site conservation., Nat Struct Biol. 6 (1999) 233–42. https://doi.org/10.1038/6675.

[5] M.M. He, A.S. Smith, J.D. Oslob, W.M. Flanagan, A.C. Braisted, A. Whitty, M.T. Cancilla, J. Wang, A.A. Lugovskoy, J.C. Yoburn, A.D. Fung, G. Farrington, J.K. Eldredge, E.S. Day, L.A. Cruz, T.G. Cachero, S.K. Miller, J.E. Friedman, I.C. Choong, B.C. Cunningham, Small-molecule inhibition of TNF-alpha., Science. 310 (2005) 1022–5. https://doi.org/10.1126/science.1116304.

[6] G.P. Vigers, L.J. Anderson, P. Caffes, B.J. Brandhuber, Crystal structure of the type-I interleukin-1 receptor complexed with interleukin-1beta., Nature. 386 (1997) 190–4. https://doi.org/10.1038/386190a0.

[7] O. Crescenzi, S. Tomaselli, R. Guerrini, S. Salvadori, A.M. D'Ursi, P.A. Temussi, D. Picone, Solution structure of the Alzheimer amyloid beta-peptide (1-42) in an apolar microenvironment. Similarity with a virus fusion domain., Eur J Biochem. 269 (2002) 5642–8. https://doi.org/10.1046/j.1432-1033.2002.03271.x.

[8] T. Lührs, C. Ritter, M. Adrian, D. Riek-Loher, B. Bohrmann, H. Döbeli, D. Schubert, R. Riek, 3D structure of Alzheimer's amyloid-β(1–42) fibrils, Proceedings of the National Academy of Sciences. 102 (2005) 17342–17347. https://doi.org/10.1073/pnas.0506723102.

[9] T.R. Hynes, M. Randal, L.A. Kennedy, C. Eigenbrot, A.A. Kossiakoff, X-ray crystal structure of the protease inhibitor domain of Alzheimer's amyloid .beta.-protein precursor, Biochemistry. 29 (1990) 10018–10022. https://doi.org/10.1021/bi00495a002.

[10] K. Fosgerau, T. Hoffmann, Peptide therapeutics: current status and future directions., Drug Discov Today. 20 (2015) 122–8. https://doi.org/10.1016/j.drudis.2014.10.003.

[11] D. Shivakumar, J. Williams, Y. Wu, W. Damm, J. Shelley, W. Sherman, Prediction of Absolute Solvation Free Energies using Molecular Dynamics Free Energy Perturbation and the OPLS Force Field., J Chem Theory Comput. 6 (2010) 1509–19. https://doi.org/10.1021/ct900587b.

[12] G.M. Sastry, M. Adzhigirey, T. Day, R. Annabhimoju, W. Sherman, Protein and ligand preparation: parameters, protocols, and influence on virtual screening enrichments., J Comput Aided Mol Des. 27 (2013) 221–34. https://doi.org/10.1007/s10822-013-9644-8.

[13] T.A. Halgren, R.B. Murphy, R.A. Friesner, H.S. Beard, L.L. Frye, W.T. Pollard, J.L. Banks, Glide: a new approach for rapid, accurate docking and scoring. 2. Enrichment factors in database screening., J Med Chem. 47 (2004) 1750–9. https://doi.org/10.1021/jm030644s.

[14] R.A. Friesner, R.B. Murphy, M.P. Repasky, L.L. Frye, J.R. Greenwood, T.A. Halgren, P.C. Sanschagrin, D.T. Mainz, Extra precision glide: docking and scoring incorporating a model of hydrophobic enclosure for protein-ligand complexes., J Med Chem. 49 (2006) 6177–96. https://doi.org/10.1021/jm051256o.

[15] M.P. Jacobson, D.L. Pincus, C.S. Rapp, T.J.F. Day, B. Honig, D.E. Shaw, R.A. Friesner, A hierarchical approach to all-atom protein loop prediction., Proteins. 55 (2004) 351–67. https://doi.org/10.1002/prot.10613.

[16] M.P. Jacobson, R.A. Friesner, Z. Xiang, B. Honig, On the role of the crystal environment in determining protein side-chain conformations., J Mol Biol. 320 (2002) 597–608. https://doi.org/10.1016/s0022-2836(02)00470-9.

[17] T. Halgren, New method for fast and accurate binding-site identification and analysis., Chem Biol Drug Des. 69 (2007) 146–8. https://doi.org/10.1111/j.1747-0285.2007.00483.x.

[18] R.A. Friesner, J.L. Banks, R.B. Murphy, T.A. Halgren, J.J. Klicic, D.T. Mainz, M.P. Repasky, E.H. Knoll, M. Shelley, J.K. Perry, D.E. Shaw, P. Francis, P.S. Shenkin, Glide: a new approach for rapid, accurate docking and scoring. 1. Method and assessment of docking accuracy., J Med Chem. 47 (2004) 1739–49. https://doi.org/10.1021/jm0306430.

[19] R. Farid, T. Day, R.A. Friesner, R.A. Pearlstein, New insights about HERG blockade obtained from protein modeling, potential energy mapping, and docking studies., Bioorg Med Chem. 14 (2006) 3160–73. https://doi.org/10.1016/j.bmc.2005.12.032.

[20] W. Sherman, H.S. Beard, R. Farid, Use of an induced fit receptor structure in virtual screening., Chem Biol Drug Des. 67 (2006) 83–4. https://doi.org/10.1111/j.1747-0285.2005.00327.x.

[21] W. Sherman, T. Day, M.P. Jacobson, R.A. Friesner, R. Farid, Novel procedure for modeling ligand/receptor induced fit effects., J Med Chem. 49 (2006) 534–53. https://doi.org/10.1021/jm050540c.

[22] G.D. Geromichalos, C.E. Alifieris, E.G. Geromichalou, D.T. Trafalis, Overview on the current status of virtual high-throughput screening and combinatorial chemistry approaches in multi-target anticancer drug discovery; Part I., J BUON. 21 (2016) 764–779. http://www.ncbi.nlm.nih.gov/pubmed/27685895.

[23] T.A. Halgren, Identifying and Characterizing Binding Sites and Assessing Druggability, J Chem Inf Model. 49 (2009) 377–389. https://doi.org/10.1021/ci800324m.

[24] D. Bashford, D.A. Case, Generalized born models of macromolecular solvation effects., Annu Rev Phys Chem. 51 (2000) 129–52. https://doi.org/10.1146/annurev.physchem.51.1.129.

[25] J. Li, R. Abel, K. Zhu, Y. Cao, S. Zhao, R.A. Friesner, The VSGB 2.0 model: a next generation energy model for high resolution protein structure modeling., Proteins. 79 (2011) 2794–812. https://doi.org/10.1002/prot.23106.

[26] W.L. DeLano, The PyMol Molecular Graphics System 0.99, (2006).

[27] D.B. Singh, M.K. Gupta, R.K. Kesharwani, K. Misra, Comparative docking and ADMET study of some curcumin derivatives and herbal congeners targeting β-amyloid, Network Modeling Analysis in Health Informatics and Bioinformatics. 2 (2013) 13–27. https://doi.org/10.1007/s13721-012-0021-7.

[28] S. Jokar, M. Erfani, O. Bavi, S. Khazaei, M. Sharifzadeh, M. Hajiramezanali, D. Beiki, A. Shamloo, Design of peptide-based inhibitor agent against amyloid-β aggregation: Molecular docking, synthesis and in vitro evaluation, Bioorg Chem. 102 (2020) 104050. https://doi.org/10.1016/j.bioorg.2020.104050.

Table S1. Binding contact residues of curcumin and V-Cur molecules in the binding site of APPI.

Target protein	Binding contact residues (Å)			
	Curcumin		V-Cur	
APPI	GLN 8A*	2.878	GLN 8A*	4.093
	ALA 9A*	3.414	ALA 9A*	3.646
	TYR 22A*	2.757	TYR 22A*	3.197
	ASP 24A*	2.834	ASP 24A*	3.397
	THR 26A*	3.116	VAL 25A	4.163
	GLU 27A	3.965	THR 26A*	2.850
	PHE 33A	4.036	GLN 8B*	2.963
	GLN 8B*	3.830	ALA 9B	3.323
	THR 11B*	3.076	THR 11B*	3.753
	ASP 24B*	4.013	TYR 22B	1.823
	VAL 25B	3.556	ASP 24B*	2.200
	THR 26B*	2.312	THR 26B*	3.353
	PRO 32B*	3.830	GLU 27B	3.647
	PHE 33B*	3.326	PRO 32B*	2.980
	PHE 34B*	2.895	PHE 33B*	3.302
			PHE 34B*	2.759

*Binding contacts common between curcumin and V-Cur

Table S2. Binding contact residues of curcumin and V-Cur molecules in the binding cavity of iNOS, TNF-α, and IL-1β target proteins (chain A of iNOS indicate the monomer structure, while chains A and B of TNF-α and IL-1β/IL-1RI, indicate the dimer TNF-α and IL-1β (A), IL-1RI (B)).

Target protein	Binding contact residues (Å)			
	Curcumin		V-Cur	
iNOS	TRP 194A	3.579	THR 121A	3.886
	ARG 199A	3.485	ALA 197A	3.320
	CYS 200A	3.964	PRO 198A	3.433
	GLY 202A	3.432	ARG 199A	3.816
	GLN 205A	3.238	CYS 200A	3.550
	SER 242A	4.014	ALA 262A	3.462
	VAL 352A*	3.979	GLN 263A	3.412
	MET 355A*	3.310	ARG 266A	3.124
	PHE 369A	3.303	TRP 346A	2.987

	ASN 370A	2.916	TYR 347A	3.253
	GLY 371A	3.285	VAL 352A*	4.056
	TRP 372A	2.890	ASN 354A	3.586
	TYR 373A*	3.984	MET 355A*	3.452
	MET 374A	3.756	TYR 373A*	2.394
	MET 434A	3.964	GLU 377A*	3.016
	GLU 377A*	4.016	ILE 378A	3.971
	ALA 439A	4.090	ASP 382A	2.278
	TRP 463A*	3.982	ARG 388A	2.945
	TYR 491A	3.758	TRP 463A*	3.910
			PHE 488A	3.551
			TYR 489A	3.777
			TYR 491A*	2.649
TNF-α	TYR 59A*	3.239	HIS 15A	3.430
	SER 60A	3.128	LEU 57A	4.007
	GLN 61A*	3.013	TYR 59A*	2.765
	TYR 119A*	3.358	GLN 61A*	2.476
	LEU 120A*	2.241	TYR 119A*	2.701
	GLY 121A*	2.966	LEU 120A*	3.963
	TYR 151A*	2.269	GLY 121A*	3.216
	ILE 155A	4.092	GLY 122A	3.739
	TYR 59B*	3.039	GLN 149A	3.269
	SER 60B*	2.502	TYR 151A*	2.201
	GLN 61B*	3.600	TYR 59B*	3.214
	TYR 119B*	3.383	SER 60B*	3.630
	LEU 120B*	2.085	GLN 61B*	4.034
	GLY 121B	3.714	TYR 119B*	3.583
	TYR 151B*	2.030	LEU 120B*	4.057
			TYR 151B*	3.744
IL-1β/IL-1RI	LEU 6A[§]	3.927	GLU 105A*[§¤]	2.971
	MET 44A	3.248	ASN 108A*[§]	2.643
	PHE 46A[§]	3.265	LYS 109A	3.787
	ILE 56A[§]	3.567	LEU 110A	3.771
	LYS 103A[§]	2.998	THR 147A	3.401
	GLU 105A*[§¤]	3.387	MET 148A*	3.360
	ILE 106A[¤]	3.160	GLN 149A	3.285
	ASN 107A	3.277	PHE 150A*	2.460
	ASN 108A*[§]	2.959	SER 152A	3.058
	MET 148A*	3.607	ARG 174B	3.164
	PHE 150A*	3.929	ILE 199B	3.627

	ASN 204B*	2.484	THR 200B	3.101
	LYS 205B	2.368	LEU 201B	3.230
	PRO 206B	3.404	GLU 202B	4.094
	GLN 236B*	3.816	ASN 204B*	3.640
	SER 238B*	2.622	GLN 236B*	4.025
	ASP 239B[§]	4.009	LEU 237B[§]	3.740
	ILE 240B[§]	4.100	SER 238B*	3.534
	ARG 271B*	3.852	GLU 265B[§]	3.066
	LYS 298B[§]	4.115	LYS 270B	3.113
	ASN 299B	3.366	ARG 271B*	4.098
	THR 300B	3.716		
	HIS 301B	3.075		

*Binding contacts common between curcumin and V-Cur

[§] Binding contacts of site B involving the third Ig-domain (D3) of IL-1RI

[¤] Binding residues of IL-1β in contact with IL-1RAcP

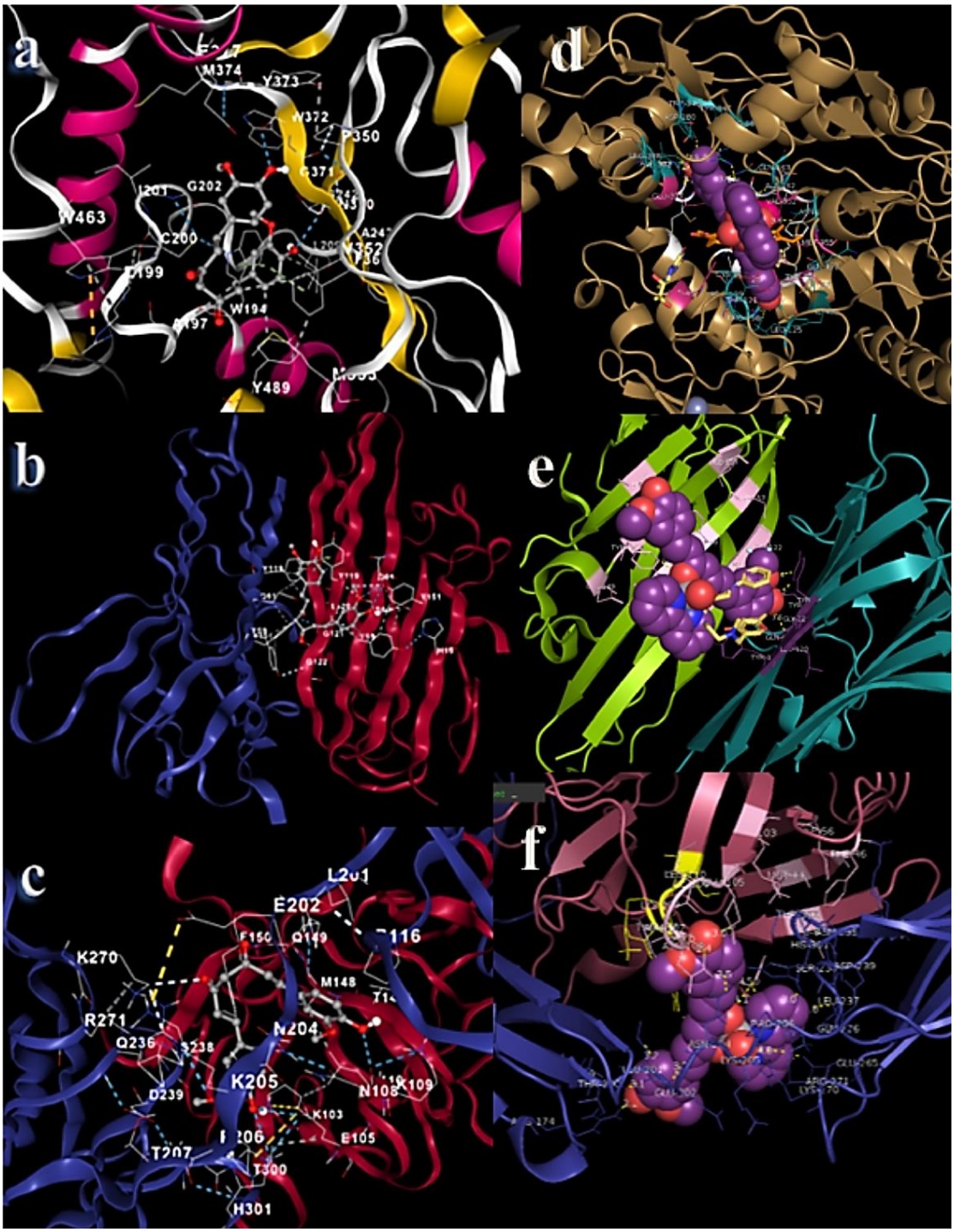

Fig. S3. Binding interaction architecture of curcumin and V-Cur in the ligand-binding site of iNOS (a and d, respectively), TNF-α (b and e, respectively), and IL-1β (c and f, respectively) target proteins.